JACS
JOURNAL OF THE AMERICAN CHEMICAL SOCIETY
Communication
pubs.acs.org/JACS

Icosahedral Platinum Alloy Nanocrystals with Enhanced Electrocatalytic Activities

Jianbo Wu,[†,‡] Liang Qi,[§] Hongjun You,[†] Adam Gross,[†] Ju Li,[§] and Hong Yang*[,†,‡]

[†]Department of Chemical Engineering, University of Rochester, Rochester, New York 14627, United States

[‡]Department of Chemical & Biomolecular Engineering, University of Illinois at Urbana−Champaign, 600 South Mathews Avenue, Urbana, Illinois 61801, United States

[§]Department of Nuclear Science and Engineering and Department of Materials Science and Engineering, Massachusetts Institute of Technology, Cambridge, Massachusetts 02139, United States

Supporting Information

ABSTRACT: This communication describes the synthesis of Pt−M (M = Au, Ni, Pd) icosahedral nanocrystals based on the gas reducing agent in liquid solution method. Both CO gas and organic surface capping agents play critical roles in stabilizing the icosahedral shape with {111} surfaces. Among the Pt−M alloy icosahedral nanocrystals generated, Pt_3Ni had an impressive ORR specific activity of 1.83 mA/cm^2_{Pt} and 0.62 A/mg_{Pt}. Our results further show that the area-specific activity of icosahedral Pt_3Ni catalysts was about 50% higher than that of the octahedral Pt_3Ni catalysts (1.26 mA/cm^2_{Pt}), even though both shapes are bound by {111} facets. Density functional theory calculations and molecular dynamics simulations indicate that this improvement may arise from strain-induced electronic effects.

Icosahedron is a polyhedral structure that exists in both organic and inorganic materials in nature.[1] The best-known icosahedral materials include carbon fullerene (C_{60}),[1a] virus,[2] and metal nanocrystals.[3] Unlike typical crystalline solids, the icosahedral particle cannot exist as a single crystal. Twin boundary defects have to be built into the icosahedral (Ih) nanoparticle.[3a] For a regular icosahedral nanocrystal, it is made of 20 tetrahedral subunits with 30 twin boundaries, resulting in a surface enclosed by 20 {111} facets.

While icosahedral nanocrystals of Ag,[4] Au,[5] and Pd[6] can be synthesized through chemical reactions in solution phase, it is rare for Pt or Pt-based metallic materials to form icosahedral nanocrystals that have multiple twin boundaries, as the internal strain energy is high for Pt twinned crystals.[3a,7] Icosahedral Pt alloy nanocrystals are not common either through solution-phase synthesis. Pt and Pd bond relatively strongly with oxygen compared with Au and Ag, which makes twin boundary defects susceptible to oxidation and greatly accelerates the etching of Pt and Pd multiple-twinned particles (MTPs).[6c,8] Therefore, a strongly reductive environment in an inert reducing gas may limit the oxidative etching of these twinned particles.[9] In this paper, we show a general method for the preparation of uniform icosahedral nanocrystals of several Pt−M (M = Au, Ni, Pd) alloys. The synthesis is based on the gas reducing agent in liquid solution (GRAILS) method,[10] which requires the use of carbon monoxide (CO) to create a strong reductive condition and organic surface capping agents. Compositions are readily controllable for these icosahedral nanocrystals, a clear affirmation of our approach.

One important characteristic of the icosahedral nanocrystals is their surfaces are bound by {111} facets exclusively. This structural feature may result in unique properties where surface atomic structures are critically important. For Pt−Ni alloys, the (111) surface is catalytically more active than other low-indexed surfaces toward the oxygen reduction reaction (ORR) which involves various types of adsorptions and reactions of hydrogen and oxygen atoms.[10a,11] The (111) surface-dominant Pt_3Ni alloy nanocrystals are still the best-known catalyst for ORR. Herewith, we show that the Pt_3Ni icosahedral nanocrystal catalyst is much more active than its {100} surface-bound cube counterpart. The ORR area specific activity is also higher than another {111} facet-enclosed octahedral nanocrystals of similar size.

The synthesis of icosahedral Pt−M alloys was carried out in nonhydrolytic solutions using the GRAILS method.[10a] In this approach, CO is used primarily as the reducing agent, but also functions as a capping agent in stabilizing selected growing surfaces.[10,12] Oleylamine (OAm) and oleic acid (OA) at a volumetric ratio of 9:1 were used in the synthetic mixture. Figure 1 shows representative transmission electron microscopy (TEM) micrographs of the icosahedral Pt_3Ni alloy nanocrystals formed using the GRAILS method.

A TEM study on a large population of icosahedral Pt_3Ni nanocrystals further shows the size and shape were uniform (Figure S1). The average size, i.e. the distance between two opposite surfaces, was 13 ± 0.3 nm (Figure 1a). The patterns of contrast in the TEM micrographs suggest the existence of twin defects in these nanocrystals. The scanning electron microscopy (SEM) image of a nanocrystal clearly shows the icosahedron shape and the characteristic 5-fold symmetry (inset of Figure 1a), which was also observed in the TEM micrograph (Figure S2). High resolution TEM (HRTEM) micrographs show the {111} and {200} planes in the tetrahedral crystal domains. The twin planes and characteristic tetrahedral structures were readily visible (Figures 1b and S3). This 5-fold symmetry and twinned boundaries were observed

Received: May 1, 2012
Published: June 27, 2012

   dx.doi.org/10.1021/ja303950v | J. Am. Chem. Soc. 2012, 134, 11880−11883

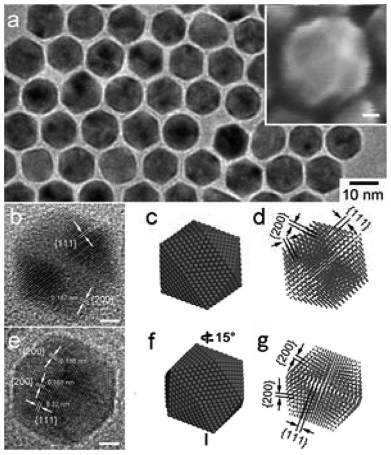

Figure 1. (a) TEM and SEM (inset) and (b–g) HRTEM micrographs, and 3D models of Pt_3Ni icosahedral nanocrystals at two different orientations, respectively. The scale bars correspond to 2 nm.

by tilting the stage under different imaging directions with more than a dozen of individual particles recorded in the HRTEM mode. The HRTEM micrograph matches very well with those schematic illustrations of the three-dimensional (3D) models of an icosahedral nanocrystal oriented with a (111) plane (Figure 1c,d). The graphics illustrated using spheres are meant to depict the surface atomic structures (Figure 1c), while those using dots facilitate the visualization of the 3D structures and twin planes (Figure 1d). If the crystal orientation with regards to the imaging beam direction changed, the patterns of light–dark contrast due to the twinning changed accordingly (Figures 1e and S3). Such contrast patterns and the 2D hexagon geometry in TEM micrographs match those simulated using the 3D models of icosahedral nanocrystals (Figure 1f,h). Thus, despite the pattern variations in contrast among these projected 2D hexagon shapes, these nanocrystals were made of the same type of tetrahedral subunits.

Scanning TEM (STEM) micrographs and energy dispersive X-ray (EDX) element mapping indicate that both Pt and Ni were distributed evenly in each nanoparticle (Figure S4a–c). Further analysis based on an SEM-EDX spectrum indicates that the composition of these icosahedral nanoparticles were close to Pt_3Ni (Figure S4d). The powder X-ray diffraction (PXRD) patterns of this sample could be indexed to (111), (200), (220), and (311) diffractions of a face-centered-cubic (fcc) structure with the peak positions in between Pt and Ni diffractions, respectively (Figure S4e). The lattice constant was calculated to be 3.83 Å, corresponding to a composition close to Pt_3Ni based on the calculation according to Vegard's law (a_{Pt} = 3.923 Å and a_{Ni} = 3.524 Å). By using the full width at half-maximum (fwhm) of the (111) diffraction and the Debye–Scherrer formulation, the crystalline domain size was calculated to be ~7 nm, which is smaller than the observed overall size of the icosahedral particles and close to the size of the tetrahedral subunits. Such a result agrees with the TEM study showing the average distance between two opposite {111} surfaces of the icosahedral particles was ~13 nm.

Besides Pt_3Ni alloy, PtAu icosahedral nanocrystals were synthesized using the GRAILS method under similar reaction conditions and with the same volumetric ratio between OAm and OA. The representative TEM micrographs show the as-made PtAu icosahedral nanocrystals were uniform (Figure 2a). The fcc crystal phase was confirmed by the XRD, and the

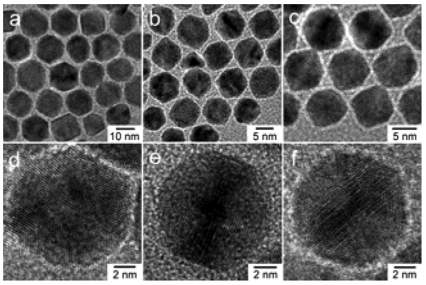

Figure 2. (a–c) TEM and (d–f) HRTEM micrographs of (a,d) PtAu, (b,e) Pt_3Pd, and (c,f) PtPd icosahedral nanocrystals.

composition of PtAu was determined by SEM-EDX (Figure S5). The typical size of these icosahedral nanocrystals was 11 ± 0.2 nm for PtAu alloy (Figure 2a). The STEM image and the Pt and Au elemental maps indicate that Pt and Au were distributed across the entire particle (Figure S6), despite the fact that Pt and Au do not readily form a solid solution in a macroscopic form.[13] Introducing a metal element that reduces the formation energy of the twin boundary, i.e. Au, might help the formation of PtAu icosahedral nanocrystals. By replacing OA with an equal volume of diphenyl ether, icosahedral nanocrystals were produced at two different Pt–Pd compositions, as confirmed by TEM micrographs showing the characteristic patterns of contrast (Figure 2b,c). HAADF-STEM and their corresponding elemental maps indicate these two Pt–Pd nanocrystals have compositions close to Pt_3Pd and PtPd, respectively (Figures S7–S9). Both (111) planes and characteristic tetrahedral domains could be readily observed in these three icosahedral Pt–M nanocrystals using HRTEM (Figure 2d–f). Small shifts of the diffraction peaks were observed at high angles in the XRD patterns for Pt–Pd alloy nanocrystals (Figure S10). The effect of composition on the shift of peak position was relatively small because the unit cell lengths for Pt and Pd lattices are very close. The formation of Pt–Pd alloy icosahedral nanocrystals with different compositions further indicates the CO-based GRAILS method is quite generic for the preparation of icosahedral nanocrystals.

The seed plays a key role in determining the shape of a nanocrystal.[6b] A seed can be a single crystal, a single twin, or multiple twins. The slow reduction process under which nucleation of metal atoms and growth of nuclei are kinetically controlled promotes the formation of twinned seeds when mild reducing agents or a low concentration of metal precursors are used.[6d,e] Icosahedral structures of selected noble metals, such as Pt, Au, and Pd, are expected to be stable below certain sizes.[14] The critical sizes are about 55 atoms for Pt (or 3 atomic layers), 147 atoms for Au, and 309 atoms for Pd metals.[4b,6d,14,15] Above these sizes, an icosahedron is less stable than a decahedron and cuboctahedron. Thus, a Pt icosahedron usually transforms into a cuboctahedron or truncated octahedron at very small sizes.[4b,16] Our experimental data on the formation of alloy icosahedral nanocrystals indicate that the size-dependent stability of the above three types of morphologies changed dramatically when two metals mixed. The relative stability among the different types of facets also changed greatly in the presence of surface capping agents. For instance, with the Pt–Pd alloy nanocrystals the icosahedral seeds bound by {111} facets were more easily formed than the {100} facets in the presence of CO and phenyl groups which preferentially stabilized the (111) surface.[10a,12b] For Pt–Ni alloys, icosahedral nanocrystals formed in a narrow composition range and were

dx.doi.org/10.1021/ja303950v | J. Am. Chem. Soc. 2012, 134, 11880–11883

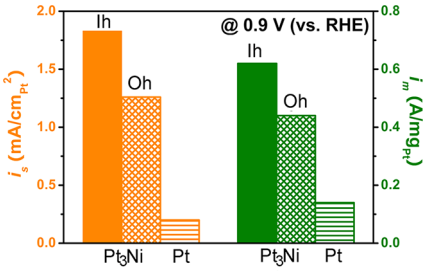

Figure 3. Mass- and area-specific activities of the Pt_3Ni icosahedral and octahedral nanocrystal and Pt reference catalysts at 0.9 V.

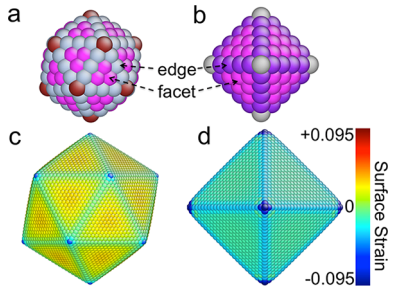

Figure 4. Atomic structures of (a) Pt icosahedral cluster with 309 atoms and (b) Pt octahedral cluster with 146 atoms. Different color means different coordination number. Surface strain fields of Pt (c) icosahedral and (d) octahedral nanocrystals with diameter of 10 nm. Color indicates strain labeled in the color map.

sensitive to the types of capping agents used. When octadecylamine and 1-adamantaneacetic acid were used, a $PtNi_3$ cubic crystal formed.[10a]

The ORR activity was measured for carbon-supported Pt_3Ni icosahedral nanocrystal electrocatalysts based on a rotating disk electrode (RDE) technique (Figure S11).[10a] The mass and area specific ORR activity were calculated by normalizing the kinetic current with the loading amount of Pt and electrochemical surface area (ECSA), respectively. The ECSA value was obtained from the hydrogen adsorption region of a cyclic voltammetry (CV) curve, between 0.05 and 0.4 V (Figure S11a). The area-specific ORR activity at 0.9 V was 1.83 mA/cm$^2_{Pt}$ for the icosahedral Pt_3Ni catalyst (Figure 3). Noticeably, this specific activity of the icosahedral Pt_3Ni alloy was an 8× improvement over that of the highly active Pt/C catalyst (TKK, d = 3 nm on Vulcan carbon, 0.20 mA/cm$^2_{Pt}$).[11c,e]

The Pt mass activity of this icosahedral Pt_3Ni catalyst was 0.62 A/mg$_{Pt}$ (Figure 3). After iR compensation, the area specific activity became 2.78 mA/cm$^2_{Pt}$ and the mass activity became 0.94 mA/g$_{Pt}$ (Figure S12 and Table S1). These ORR activities of the icosahedral Pt_3Ni catalyst are better than those of the other {111} faceted Pt_3Ni/C catalysts, and dendritic Pt−Pd/C catalysts tested under similar conditions.[10a,11c,d,17] The half wave potential of icosahedra was 0.90 vs 0.88 V, indicating a shift of 15 mV (Figure S11b, inset). The onset potentials between icosahedral and octahedral Pt_3Ni catalysts, both with the {111} surfaces, were relatively small and ∼4 mV (Figure S13). To verify the ORR catalytic pathways of octahedral and icosahedral Pt_3Ni, we used a rotating ring-disk electrode (RRDE) to monitor the formation of peroxide (H_2O_2) during the ORR process (Figure S14).[18] The measured H_2O_2 yields are below 11% for the octahedron and 3% for the icosahedron at the potential range of 0.10−0.80 V, suggesting that the {111} facets on icosahedral Pt_3Ni might restrain the generation of H_2O_2. Interestingly, the activity of icosahedral Pt_3Ni catalysts was also 50% higher than that of the octahedral with a similar size (Figure 3),[10a] despite the fact that both shapes are bound by {111} facets (Figure S15). This observation suggests that the facet is not the only major factor to determine the catalytic activity of nanocrystals.

To understand the origin of the observed difference in activity between icosahedral and octahedral nanoparticles, both of which are bounded by {111} facets, we performed density functional theory (DFT) calculations. As the surfaces of Pt alloy catalysts under acidic conditions are made exclusively of Pt, pure Pt shapes were used in the simulation for simplicity. Generally, coordination numbers (CN) of atoms on the edge of icosahedral and octahedral nanoparticles are 8 and 7, respectively, while on {111} facets the CN is 9 (Figure 4a,b). Atoms with a lesser CN number would have stronger adsorption strengths, resulting in a different catalytic activity. However, DFT calculations show that the adsorption energy differences of a hydroxyl (OH), an important ORR reaction intermediate, on the edge of icosahedral and octahedral Pt nanoparticles is only 0.05 eV (details in Supporting Information (SI), Figure S16).[19] Using atomic models of nanoparticles with a diameter of 10 nm,[20] we found the percentage of edge atoms relative to all atoms on the surface is only 14% for icosahedral and 7% octahedral geometry. So it is unlikely that such a small difference in adsorption energies on a small portion of surface atoms can result in an observable large change in catalytic activities. This assertion is supported by our recent theory of reactivity sensitivity to material energetics and microkinetic modeling, where we found the true reactivity sensitivity is much smaller than what the naive Arrhenius law (exp(0.05 eV/k_BT_{room})) would have predicted, due to surface coverage effects.[21]

Another possible factor is the elastic strain,[22] which is particularly pronounced for an icosahedral nanoparticle with the high density of twin. We use molecular dynamics (MD) simulations to obtain the strain fields on the surface of icosahedral and octahedral Pt nanocrystals with a diameter of 10 nm (details in SI).[23] As shown in Figure 4c,d, the surface strain on an icosahedral nanoparticle is tensile (averaging +1.6%), while it is compressive (averaging −1.6%) on an octahedral nanoparticle. Such surface strain differences (3%−4%) could significantly change the ORR catalytic activity, which was observed by studies on core−shell Pt−Cu nanoparticles.[24] The direct role of surface strain is to tune the electronic structure of surface atoms by shifting their d-band center, which results in the variations of adsorption strength.[25] Our DFT calculations indeed show that there is a large difference in the d-band center (0.36 eV) and hydroxyl adsorption energy (0.26 eV) even for atoms on the {111} facet of small Pt icosahedral and octahedral nanoparticles (Figures S16 and S17).

More calculations suggest that although the absolute strain values may change, differences in strain, electronic structures, and adsorption energies between their icosahedral and octahedral nanocrystals should have similar trends for Pt_3Ni and other bimetallic alloys, such as Al_3Cu (details in SI, Figures S18−S21), because they are determined by the icosahedral geometry, namely the need to elastically stretch the subunits to meet at the twin boundaries and compensate for misfit angles between the 20 subunits, which does not exist in the octahedral single crystal. Previous theoretical studies on the periodic surface model suggests that the adsorption strength on the (111) surface of Pt_3Ni with a pure Pt top layer is slightly weaker

dx.doi.org/10.1021/ja303950v | J. Am. Chem. Soc. 2012, 134, 11880−11883

than the value to reach possible maximum ORR activity,[26] and increasing/decreasing the tensile/compressive strain would increase the adsorption strengths because it shifts up d-band center.[25b] These tendencies are consistent with the activity and strain changes on both pure Pt and bimetallic alloy icosahedral and octahedral nanoparticles observed in our studies.

In summary, several types of Pt alloy icosahedral nanocrystals have been synthesized based on the GRAILS method. Our experimental results and theoretical studies together suggest that the diffuse elastic strain seen on the surface, induced by stretching the 20 tetrahedra, should be the dominant factor for the increase in ORR activity of the Pt_3Ni icosahedral nanoparticle relative to its octahedral counterpart. It provides us with a new route for controlling the catalytic activity by manipulating the nanoparticle geometry.[11a,27]

■ ASSOCIATED CONTENT

Ⓢ Supporting Information

This material is available free of charge via the Internet at http://pubs.acs.org.

■ AUTHOR INFORMATION

Corresponding Author

hy66@illinois.edu

Notes

The authors declare no competing financial interest.

■ ACKNOWLEDGMENTS

This work was supported in part by the NSF (DMR-0449849 to H.Y., DMR-1120901 to J.L.) and AFOSR (FA9550-08-1-0325 to J.L.).

■ REFERENCES

(1) (a) Kroto, H. W.; Allaf, A. W.; Balm, S. P. *Chem. Rev.* **1991**, *91*, 1213. (b) Teo, B. K.; Zhang, H. *Coord. Chem. Rev.* **1995**, *143*, 611. (c) Korbe, S.; Schreiber, P. J.; Michl, J. *Chem. Rev.* **2006**, *106*, 5208.

(2) Voss, J. E.; Vaney, M. C.; Duquerroy, S.; Vonrhein, C.; Girard-Blanc, C.; Crublet, E.; Thompson, A.; Bricogne, G.; Rey, F. A. *Nature* **2010**, *468*, 709.

(3) (a) Xia, Y.; Xiong, Y. J.; Lim, B.; Skrabalak, S. E. *Angew. Chem., Int. Ed.* **2009**, *48*, 60. (b) Hakkinen, H.; Moseler, M.; Kostko, O.; Morgner, N.; Hoffmann, M. A.; von Issendorff, B. *Phys. Rev. Lett.* **2004**, *93*, 093401. (c) Chen, F. Y.; Johnston, R. L. *ACS Nano* **2008**, *2*, 165.

(4) (a) Tsuji, M.; Ogino, M.; Matsuo, R.; Kumagae, H.; Hikino, S.; Kim, T.; Yoon, S. H. *Cryst. Growth Des.* **2010**, *10*, 296. (b) Baletto, F.; Mottet, C.; Ferrando, R. *Phys. Rev. B* **2001**, *63*, 155408.

(5) (a) Goubet, N.; Ding, Y.; Brust, M.; Wang, Z. L.; Pileni, M. P. *ACS Nano* **2009**, *3*, 3622. (b) Yavuz, M. S.; Li, W. Y.; Xia, Y. N. *Chem.—Eur. J.* **2009**, *15*, 13181. (c) Xu, J.; Li, S. Y.; Weng, J.; Wang, X. F.; Zhou, Z. M.; Yang, K.; Litt, M.; Chen, X.; Cui, Q.; Cao, M. Y.; Zhang, Q. Q. *Adv. Funct. Mater.* **2008**, *18*, 277. (d) Yao, H.; Minami, T.; Hori, A.; Koma, M.; Kimura, K. *J. Phys. Chem. B* **2006**, *110*, 14040.

(6) (a) Lim, B.; Jiang, M. J.; Tao, J.; Camargo, P. H. C.; Zhu, Y. M.; Xia, Y. N. *Adv. Funct. Mater.* **2009**, *19*, 189. (b) Xiong, Y. J.; Xia, Y. N. *Adv. Mater.* **2007**, *19*, 3385. (c) Xiong, Y. J.; McLellan, J. M.; Yin, Y. D.; Xia, Y. N. *Angew. Chem., Int. Ed.* **2007**, *46*, 790. (d) Lim, B.; Xiong, Y. J.; Xia, Y. N. *Angew. Chem., Int. Ed.* **2007**, *46*, 9279. (e) Li, C. C.; Sato, R.; Kanehara, M.; Zeng, H. B.; Bando, Y.; Teranishi, T. *Angew. Chem., Int. Ed.* **2009**, *48*, 6883.

(7) (a) Dai, Z. R.; Sun, S. H.; Wang, Z. L. *Surf. Sci.* **2002**, *505*, 325. (b) Maksimuk, S.; Teng, X.; Yang, H. *J. Phys. Chem. C* **2007**, *111*, 14312. (c) Tian, N.; Zhou, Z. Y.; Sun, S. G.; Ding, Y.; Wang, Z. L. *Science* **2007**, *316*, 732. (d) Peng, Z. M.; Yang, H. *Nano Today* **2009**, *4*, 143.

(8) (a) Wang, Z. L. *J. Phys. Chem. B* **2000**, *104*, 1153. (b) Wiley, B.; Herricks, T.; Sun, Y. G.; Xia, Y. N. *Nano Lett.* **2004**, *4*, 1733. (c) Niehus, H.; Comsa, G. *Surf. Sci.* **1980**, *93*, L147. (d) Voogt, E. H.; Mens, A. J. M.; Gijzeman, O. L. J.; Geus, J. W. *Surf. Sci.* **1997**, *373*, 210.

(9) Xiong, Y. J.; Chen, J. Y.; Wiley, B.; Xia, Y. N. *J. Am. Chem. Soc.* **2005**, *127*, 7332.

(10) (a) Wu, J. B.; Gross, A.; Yang, H. *Nano Lett.* **2011**, *11*, 798. (b) Kang, Y.; Ye, X.; Murray, C. B. *Angew. Chem., Int. Ed.* **2010**, *49*, 6156.

(11) (a) Wagner, F. T.; Lakshmanan, B.; Mathias, M. F. *J. Phys. Chem. Lett.* **2010**, *1*, 2204. (b) Stamenkovic, V. R.; Fowler, B.; Mun, B. S.; Wang, G. F.; Ross, P. N.; Lucas, C. A.; Markovic, N. M. *Science* **2007**, *315*, 493. (c) Wu, J.; Zhang, J.; Peng, Z.; Yang, S.; Wagner, F. T.; Yang, H. *J. Am. Chem. Soc.* **2010**, *132*, 4984. (d) Zhang, J.; Yang, H. Z.; Fang, J. Y.; Zou, S. Z. *Nano Lett.* **2010**, *10*, 638. (e) Gasteiger, H. A.; Kocha, S. S.; Sompalli, B.; Wagner, F. T. *Appl. Catal., B* **2005**, *56*, 9.

(12) (a) Wu, B. H.; Zheng, N. F.; Fu, G. *Chem. Commun.* **2011**, *47*, 1039. (b) Schauermann, S.; Hoffmann, J.; Johanek, V.; Hartmann, J.; Libuda, J.; Freund, H. J. *Angew. Chem., Int. Ed.* **2002**, *41*, 2532. (c) Eichler, A. *Surf. Sci.* **2002**, *498*, 314. (d) Somorjai, G. A.; Li, Y. *Introduction to Surface Chemistry and Catalysis*, 2nd ed.; John Wiley & Sons: Hoboken, NJ, 2010.

(13) (a) Bond, G. C. *Platinum Met. Rev.* **2007**, *51*, 63. (b) Luo, J.; Maye, M. M.; Petkov, V.; Kariuki, N. N.; Wang, L. Y.; Njoki, P.; Mott, D.; Lln, Y.; Zhong, C. J. *Chem. Mater.* **2005**, *17*, 3086. (c) Lu, Y. C.; Xu, Z. C.; Gasteiger, H. A.; Chen, S.; Hamad-Schifferli, K.; Shao-Horn, Y. *J. Am. Chem. Soc.* **2010**, *132*, 12170. (d) Peng, Z. M.; Yang, H. *Nano Res.* **2009**, *2*, 406.

(14) Baletto, F.; Ferrando, R. *Rev. Mod. Phys.* **2005**, *77*, 371.

(15) Baletto, F.; Ferrando, R.; Fortunelli, A.; Montalenti, F.; Mottet, C. *J. Chem. Phys.* **2002**, *116*, 3856.

(16) (a) Ikeshoji, T.; Torchet, G.; de Feraudy, M. F.; Koga, K. *Phys. Rev. E* **2001**, *63*, 031101. (b) Feigl, C.; Grochola, G.; Opletal, G.; Snook, I. K.; Russo, S. P. *Chem. Phys. Lett.* **2009**, *474*, 115. (c) Lu, H. M.; Li, P. Y.; Cao, Z. H.; Meng, X. K. *J. Phys. Chem. C* **2009**, *113*, 7598. (d) Kim, D. H.; Kim, H. Y.; Ryu, J. H.; Lee, H. M. *Phys. Chem. Chem. Phys.* **2009**, *11*, 5079. (e) Schooss, D.; Blom, M. N.; Parks, J. H.; von Issendorff, B.; Haberland, H.; Kappes, M. M. *Nano Lett.* **2005**, *5*, 1972.

(17) (a) Lim, B.; Jiang, M. J.; Camargo, P. H. C.; Cho, E. C.; Tao, J.; Lu, X. M.; Zhu, Y. M.; Xia, Y. A. *Science* **2009**, *324*, 1302. (b) Peng, Z. M.; Yang, H. *J. Am. Chem. Soc.* **2009**, *131*, 7542.

(18) (a) Paulus, U. A.; Schmidt, T. J.; Gasteiger, H. A.; Behm, R. J. *J. Electroanal. Chem.* **2001**, *495*, 134. (b) Sethuraman, V. A.; Weidner, J. W.; Haug, A. T.; Motupally, S.; Protsailo, L. V. *J. Electrochem. Soc.* **2008**, *155*, B50.

(19) Kresse, G.; Furthmuller, J. *Phys. Rev. B* **1996**, *54*, 11169.

(20) Glasner, D.;Frenkel, A. I. In *X-Ray Absorption Fine Structure-XAFS13*; Hedman, B. P. P., Ed.; 2007; Vol. 882, pp 746−748.

(21) (a) Qi, L.; Li, J. *J. Catal.* **2012** (JCAT-11-642R2). (b) Hansgen, D. A.; Vlachos, D. G.; Chen, J. G. *Nat. Chem* **2010**, *2*, 484. (c) Grabow, L. C.; Hvolbæk, B.; Nørskov, J. K. *Top. Catal.* **2010**, *53*, 298.

(22) Zhu, T.; Li, J. *Prog. Mater. Sci.* **2010**, *55*, 710.

(23) Foiles, S. M.; Baskes, M. I.; Daw, M. S. *Phys. Rev. B* **1986**, *33*, 7983.

(24) Strasser, P.; Koh, S.; Anniyev, T.; Greeley, J.; More, K.; Yu, C.; Liu, Z.; Kaya, S.; Nordlund, D.; Ogasawara, H.; Toney, M. F.; Nilsson, A. *Nat. Chem.* **2010**, *2*, 454.

(25) (a) Hammer, B.; Norskov, J. K. 1995, *343*, 211. (b) Hammer, B.; Norskov, J. K. In *Advances in Catalysis, Vol 45: Impact of Surface Science on Catalysis*; Gates, B. C., Knözinger, H., Eds.; 2000; Vol. 45, pp 71−129.

(26) Stamenkovic, V.; Mun, B. S.; Mayrhofer, K. J. J.; Ross, P. N.; Markovic, N. M.; Rossmeisl, J.; Greeley, J.; Norskov, J. K. *Angew. Chem., Int. Ed.* **2006**, *45*, 2897.

(27) (a) Somorjai, G. A.; Frei, H.; Park, J. Y. *J. Am. Chem. Soc.* **2009**, *131*, 16589. (b) Greeley, J.; Stephens, I. E. L.; Bondarenko, A. S.; Johansson, T. P.; Hansen, H. A.; Jaramillo, T. F.; Rossmeisl, J.; Chorkendorff, I.; Norskov, J. K. *Nat. Chem.* **2009**, *1*, 552.